2008

Detection of organosilanes with surface enhanced infrared spectroscopy

Anh Duong
San Jose State University

DETECTION OF ORGANOSILANES WITH SURFACE ENHANCED INFRARED SPECTROSCOPY

A Thesis

Presented to

The Faculty of the Department of Chemistry

San Jose State University

In Partial Fulfillment

of the Requirements for the Degree

Master of Science

by

Anh Duong

August 2008

APPROVED FOR THE DEPARTMENT OF CHEMISTRY

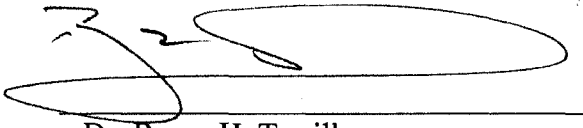

Dr. Roger H. Terrill

Dr. Patrick E. Fleming

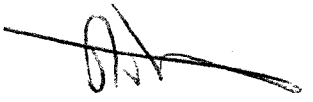

Dr. Gilles Muller

APPROVED FOR THE UNIVERSITY

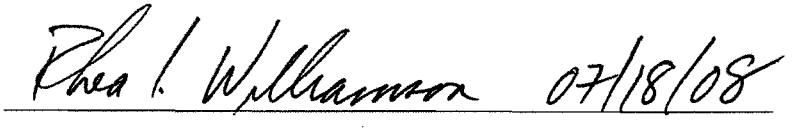

ABSTRACT

DETECTION OF ORGANOSILANES WITH SURFACE ENHANCED INFRARED SPECTROSCOPY

by Anh Duong

Infrared transmission spectra of 1 nm thick organic films were studied with and without the aid of a 5 nm thick Au island film enhancement layer. It is estimated that absorbance intensities for these molecules were about 100 to 200 times higher when they were deposited onto Au films. When the Au film is annealed at 250°C the absorbance of these molecules decreased. The smaller islands in the un-annealed Au films were more active enhancers of the IR absorption. Given the approximate concentration of the molecules within the molecular film and assuming that the extinction coefficients are the same in solution and in the film, the apparent thickness can be calculated. This thickness exceeds the measured thickness by 10 - 300 times. Even accounting for some additional adsorbed material using a simple model of the surface, this thickness is greater 5 - 150 times, than the true thickness.

ACKNOWLEDGEMENTS

I thank my research advisor, Dr. Terrill, for his guidance through the course of my research work. Also, I am thankful for his valuable comments and suggestions regarding the writing of this thesis.

I thank Dr. Patrick Fleming and Dr. Roy Okuda for being my committee members and for their advice and assistance during the critical time of composing this thesis.

I would like to thank Dr. Gilles Muller for readily accepting my request to be part of my thesis committee on short notice and for his valuable input.

I would also like to thank my husband/buddy who gave me support through the course of my research and studies.

TABLE OF CONTENTS

LIST OF FIGURES

LIST OF TABLES

1. INTRODUCTION

1.1 Research Goal

The purpose of this research is to develop a protocol for detecting and characterizing ultrathin molecular films comprising single monolayers or hybrid bilayers using surface enhanced infrared absorbance (SEIRA) spectroscopy. Our basic hypothesis is that a simple gold (Au) coating protocol can transform a silicon (Si) wafer support into a sensitive infrared (IR) detector for the analysis of ultrathin organic films. Specifically, we propose that this 5 nm Au coating will increase the IR absorbance signal of a molecular layer adsorbed to it to such an extent as to render it conveniently detectable when interrogated in a simple transmission mode. Proof of this will be given by employing a 1 nm thick physisorbed layer, a 1 nm thick chemisorbed layer and a roughly 2 nm thick chemisorbed bilayer.

The phenomenon of SEIRA is a strong enhancement in the absorption of infrared light by molecules deposited onto certain metal nanoparticle films.[1] The 'surface enhancement' is believed to be due to interactions between the molecular oscillators that absorb IR radiation and the localized surface plasmons excited in small metal particles by the IR radiation. Enhancement is also believed to be due to chemical interactions between the adsorbates and the metal surface. The magnitude of the enhancement depends strongly on both the Au particle film morphology and the analyte molecule's reactivity with the Au. In this study the adsorbates examined include *p*-nitrobenzoic acid (*p*-NBA), mercaptoalkyl acids such as 3-mercaptopropinoic acid (MPA), 11-mercaptoundecanoic acid (MUA), 16-mercaptohexadecanoic acid (MHA), and several

organosilanes such as N-(2-aminoethyl)-3-aminopropyltrimethoxysilane, vinyldimethylsilane, and phenyldimethylsilane bound to an 11-mercaptoundencanoic acid (MUA) layer. Chemical structures of these molecules are showed in Table 1 below

The Au films were deposited on a Si substrate using thermal evaporation and sputtering methods. Using SEIRA in the transmission mode enabled the detection and spectroscopic distinction of the chemical species *p*-NBA, MUA, vinyldimethylsilane, and phenyldimethylsilane bound to MUA.

Table 1. Chemical names and structures of molecules used during SEIRA experiment.

Chemical Name	Structure
p- nitrobenzoic acid (*p*-NBA)	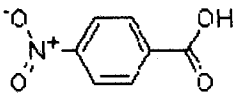
3-mercaptopropanoic acid (MPA)	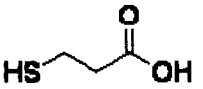
11-mercaptoundecanoic acid (MUA)	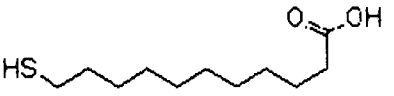
16-mercaptohexadecanoic acid (MHA)	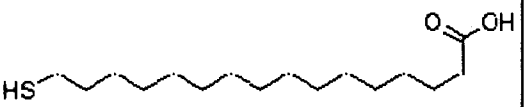
N-(2-aminoethyl)-3-aminopropyltrimethoxy silane (AEAP-TM)	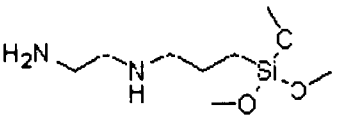
vinyldimethylchlorosilane (VDM-Cl)	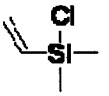
phenyldimethylchlorosilane (PhDM-Cl)	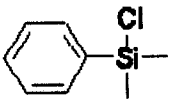

These molecules were chosen for the following reasons. Firstly, there are several comparative reports of SEIRA using *p*-NBA so a baseline comparison of SEIRA efficiency could be established. Secondly, MUA forms a well-defined monomolecular layer that can be studied with little or no ambiguity about the molecular coverage. Thirdly, MUA comprises a base layer to which the spectrally distinct secondary layer silanes could be bound. This provides a test of the sensitivity of SEIRA to layers slightly physically removed from the Au surface.

1.2 The SEIRA Phenomenon

The first report of the surface enhanced infrared absorption phenomenon was made by Hartstein[1] in early 1980, where he observed the signal of *p*-NBA deposited on a thin layer of silver to be more than 30 times stronger than *p*-NBA deposited onto the same substrate but without the thin layer of silver.[1-5] This effect came to be known as SEIRA. Some twenty years later it is now largely accepted that both electromagnetic and chemical contributions underpin the effect. The major contributors to the SEIRA effect are believed to be a) the structure of the metal enhancing surface (i.e., the shapes and sizes of the constituent metal particles), b) the interactions between the analyte molecules and the metal layer (i.e., possible chemical bonds), and c) the type of metal (typically gold, silver, platinum, or copper, based on their complex optical constants).[6, 7] Also, because of the electrical permittivity of the metal, the enhancement is expected to be greatest when the molecular layer is ordered in such a way as to put a substantial component of the vibrational transition dipole moment along the surface normal.[6]

SEIRA has more recently become an active area of research due to its sensitivity in measuring layers of atomic dimension which are important for many applications such as microelectronics, biochemical sensors, and optical memory.[6-11]

SEIRA is a simple method, where a thin layer (20 - 200 Å) of metal (e.g., Au, Ag, Pt, or Sn) is deposited onto a substrate followed by the deposition of the analyte. Such extremely thin thermally evaporated or sputtered thin films of metals tend to have an "islanded" structure which is crucial to the electromagnetic resonance phenomenon.[1] Figure 1 is a schematic of the substrate, metal island film and analyte.

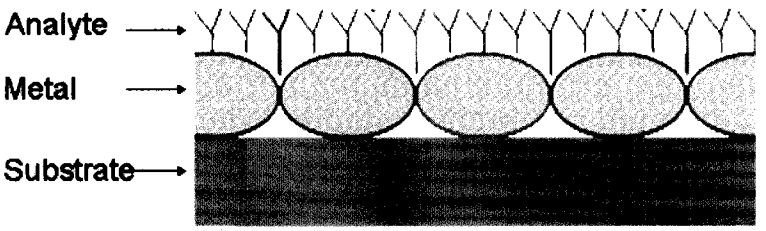

Figure 1. The model of the metal-analyte.

The transmission or reflection of IR radiation is then measured first of the clean island film for reference and then of the islands plus analyte. The resulting absorbance spectrum closely resembles that of the free analyte but with certain bands strongly enhanced. In the infrared region, the incident radiation has a wavelength much larger than the 1 - 2 nm metal islands. This favors an electromagnetic resonance, known as a Mie resonance that causes the incident radiation to induce an oscillating dipole in the

metal islands, which in turn causes a strong electromagnetic field around the metal islands.[12]

Mie theory or Lorenz-Mie theory is a complete solution for the scattering of electromagnetic radiation by spherical particles. It calculates the extinction cross section (σ), when the size of the particles is less than 20nm.[13-15] The theoretical extinction cross section equation for very small spherical particles is listed in equation 1 below:

$$\sigma = \frac{9 \cdot V \cdot \varepsilon_M^{3/2}}{c} \cdot \frac{\omega \cdot \varepsilon''(\omega)}{(\varepsilon(\omega)' + 2 \cdot \varepsilon_M)^2 + \varepsilon''(\omega)^2} \qquad (1)$$

Where σ is the scattering cross section

V is the particle volume

ε_M is the dielectric constant of the medium

c is the speed of light

ω is the light frequency

Note that a resonance condition is fulfilled when $\varepsilon(\omega)' = -2\,\varepsilon_M$, hence resonance is dependent on both the substrate and solution media and the metal. This condition may be used as a guide to determine what light frequency ranges will lead to spectral enhancement phenomena like surface enhanced Raman scattering (SERS) and SEIRA but computation of the SEIRA effect is still the subject of research. The full set of equations for Mie scattering is extensive and governs the radial distribution of scattered light intensity and may also be solved for local electric field strengths. For nanoparticle films the local dielectric function (ε_M) is a composite of the substrate, solution and metal

particles and must be approximated with effective medium theory though even with such approximations interparticle electromagnetic coupling is still largely unaccounted for.[14,15]

It is generally accepted however that molecules either physically or chemically adsorbed on the surface of the metal couple to this electromagnetic field via their own vibrationally induced dipoles as in the case of normal IR light absorption. But because of the Mie resonance in the metal particles the local electric field strengths can be greatly magnified, and the corresponding absorptions appear to be enhanced by a factor roughly equal to the square of the ratio of the free-space and local plasmonic electric field strength.[12] Also, because the molecules experiencing SEIRA are generally adsorbed to a metal surface,[1,6,16] they will tend also to follow the surface selection rule which states that for a given vibrational mode to be IR-active it must have a component of its transition dipole moment that is perpendicular to the local metal surface (along the local surface normal), which favors certain modes over others.[17] This leads to a different looking spectrum because band intensities are redistributed, but band positions appear to be largely conserved.

Figure 2 depicts approximately the electromagnetic field induced by the radiation as it distributes about the metal island. The substrate in this Figure is represented by the blue block which may be, for example, silicon, germanium, ZnSe or another IR transparent material. The gold oval represents the metal island which can be one of a variety of metals including gold, silver, copper, and platinum. Resonant coupling of the incident electromagnetic radiation to the free electrons in the metal causes a strong electromagnetic field to accumulate at the metal surface. The electromagnetic field is

represented by dotted lines. Note that the electric field lines are largely constrained to the metal surface normal as they exit the metal particle.

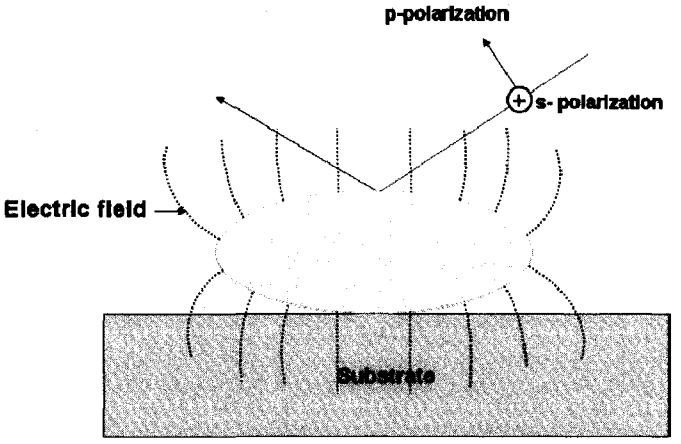

Figure 2. Electromagnetic field of metal island.

Since electric fields at metal surfaces only lie only along the surface normal, only those vibrations that produce oscillating dipoles with components that are perpendicular to the surface exhibit the SEIRA effect. This phenomenon is expressed in the following equation.[2]

$$I \sim \Gamma (d\mu / dQ)^2 |E|^2 \cos^2\theta \sim \Gamma \cos^2\theta \qquad (2)$$

Where I is the relative intensity of the absorption

Γ is the surface concentration of absorbers

θ is the angle between the dipole moment derivatives of the vibrational mode and the surface normal,

$(d\mu / dQ)^2$ is the amplitude of the dynamic dipole and

$|E|^2$ is the square of the electric field that excites the molecule.

Figure 3 illustrates the surface selection rule as it might apply to the symmetric stretching mode of the NO_2 group of an adsorbed *p*-NBA molecule. In Figure 3a, the *p*-NBA molecule is oriented such that the symmetric NO_2 stretch (ν_s NO_2) has a dynamic dipole moment that lies along the surface normal. The ν_s NO_2 mode actually has two dipolar components, a and b, that oscillate in phase yielding a vector sum c. In Figure 3a, this resultant dipole lies along the surface normal, coincident with the local electric field driven by the IR radiation which is also confined to the surface normal. In Figure 3b the effect of a change in molecular orientation is illustrated. In this case both the major axis of the molecule and the dynamic dipole moment of the NO_2 group both lie parallel to the metal surface. This dipole moment is now orthogonal to the incident IR field and therefore this mode is expected to be IR silent.[5] Using equation 2 above can sometimes yield estimates of the orientation of molecules at the metal surface.[2]

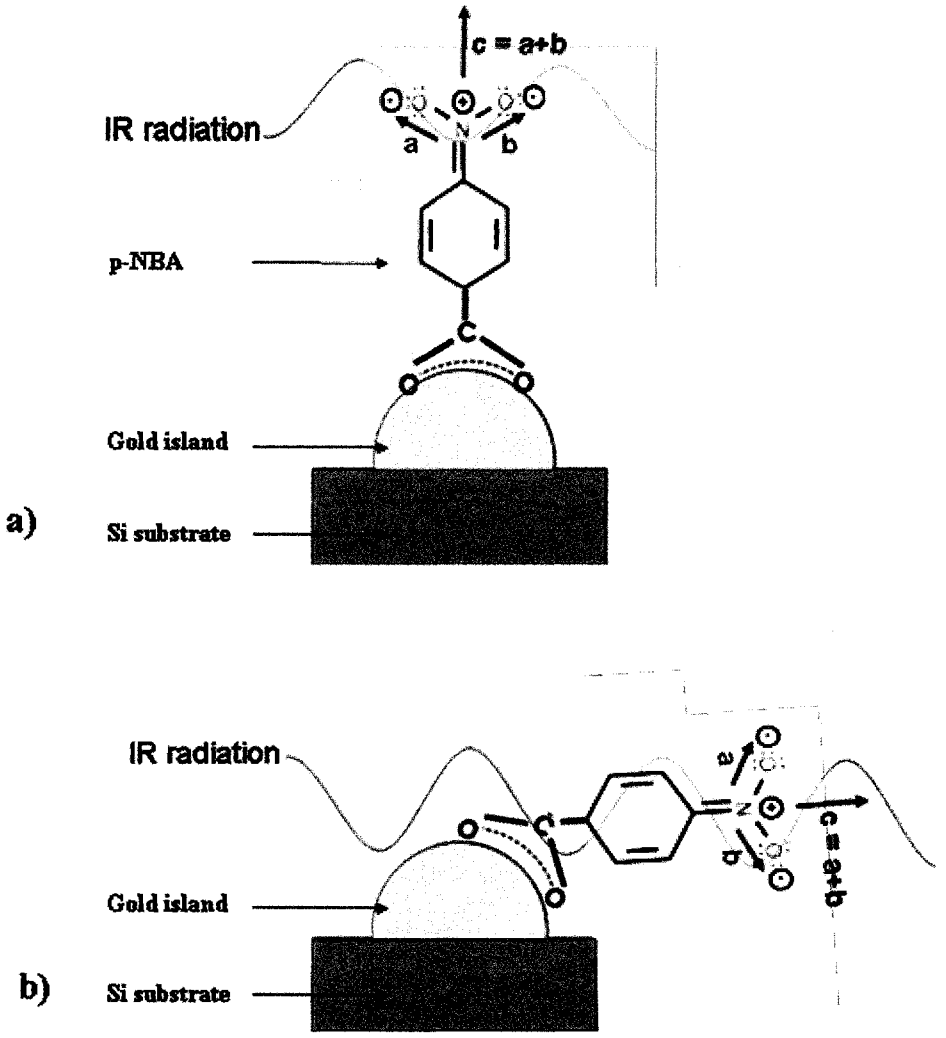

Figure 3. Effect of molecular orientation on SEIRA enhancement where a) is IR active and b) is IR inactive.

As implied above, most research supports the conclusion that the SEIRA mechanism is electromagnetic in origin.[1,6,7,16] However molecular structure and polarizablity of the absorbate clearly also play an important role in SEIRA enhancement because of the strikingly different levels of enhancement exhibited by different vibrational modes. This chemical effect was described by Badilescu and co-workers who observed a pronounced enhancement for molecules containing functional groups such as carboxylic acid and nitro groups.[13] The underpinnings of this chemical effect were further explored by Osawa and co-workers who examined the role of charge transfer between the adsorbate and metal determining SEIRA intensities. They described SEIRA as due to "a vibronic union of vibrational modes with charge-transfer excitations between the metal surface and the analyte molecule such as *p*-NBA."[18] In this framework, SEIRA is thought to be augmented by chemical interactions between the molecule when the metal surface induces a change in the vibrational polarizability (also known as the vibrational hyperpolarizability) of the molecule. This hypothesis is supported by the large SEIRA enhancement (~ 20 to 30 fold) observed for CO bound to silver because binding is known to greatly increase the vibrational hyperpolarizability of bound CO relative to free CO.[5,8,16] Merklin and Griffiths subsequently corroborated these studies using a series of the nitrophenols because the nitro-group is strongly coupled electronically to the Ag surface. The nitrophenols are believed to undergo donor-acceptor interactions with Ag upon chemisorption. Accordingly the vibrational modes associated with the nitro group exhibit a large SEIRA enhancement factor of roughly 20 to 30.[5]

1.3 Experimental Factors that Affect SEIRA Enhancement

Among those parameters conveniently accessible to the experimentalist are variation of the substrates, metal and metal deposition parameters. Many different IR transparent substrates have been used to study SEIRA enhancement including Ge,[7] CaF_2,[3] and Si.[19] The metal layers that have been studied include gold, silver,[3-5] platinum,[20] copper,[5] and ruthenium.[21] The most common metal used is gold since it is not easily oxidized. There are also several different ways to deposit the metal films, including resistive thermal evaporation, physical vapor deposition, and electrochemical deposition.[19,21] In order to achieve the best SEIRA results optimization of metal deposition rate, film thickness (20 to 200 Å), temperature and cleanliness of the substrate before and after the deposition is required. The enhancement factors appear to be largest (up to several hundred fold) when metal islands are densely aggregated but not interconnected.[22,23]

Many studies also have been done to improve enhancement by varying factors such as surface roughness,[24] surface irregularities,[8] molecular orientation,[23] metal film thickness,[25,26] and metal-molecule-metal sandwich configurations.[27] Table 2 lists the relative enhancement factors found for these conditions. Recently several studies have shown the importance of having alkanethiol self-assembled monolayers (SAMs) on the metal surface as a base for building another layer as an example.[28-31] Other studies demonstrated that optimal enhancement was observed for grazing angle external reflection at ~ 80° and for metal films of approximately 4 - 10 nm thickness (p- and s-polarized light gave similar results).[4,10,32] For external reflection the incident angle is

important because it dictates various parameters such as the interfacial reflectivities (and therefore the effective absorbing path length of the radiation through the surface layer), as well as introducing a polarization dependence to the phenomenon as is the case in any light reflection.

Table 2. Relative enhancement factor after metal surface and configuration being modified.

Main Parameter Studied	Metal Type	Molecule	Relative Enhancement Factor	Reference
surface roughness	Ag	octanethiol	5	14
surface irregularities	Ag/ Cu	*p*-NBA	5 - 30	15
molecular orientation	Au	benzenethiol	-	13
metal film thickness	Au	4-pyridinethiol	70	16
metal-molecule-metal sandwich structures	Au	4-pyridinethiol	59	16

It is possible to approximate the granular metal film as a pseudo-homogeneous phase and to then take advantage of the straight-forward Fresnel calculations for predicting approximate SEIRA spectra.[16] The Fresnel equations assume that the materials are *non-magnetic*, and may be used to calculate R_S , R_P, T_S , and T_P where R is the reflection coefficient and T is the transmission coefficient for p- and s-polarized incident rays. For a single reflection the Fresnel equations may be stated succinctly, as below. If the incident light is s-polarized, the reflection coefficient is given by equation 3 below:

$$R_s = \left[\frac{\sin(\theta_t - \theta_i)}{\sin(\theta_t + \theta_i)}\right]^2 = \left[\frac{n_1 \cos(\theta_i) - n_2 \cos(\theta_t)}{n_1 \cos(\theta_i) + n_2 \cos(\theta_t)}\right]^2 \quad (3)$$

Where θ_t can be derived from θ_i by Snell's law.

If the incident light is p-polarized, the R is given by equation 4 below:

$$R_p = \left[\frac{\tan(\theta_t - \theta_i)}{\tan(\theta_t + \theta_i)}\right]^2 = \left[\frac{n_1 \cos(\theta_t) - n_2 \cos(\theta_i)}{n_1 \cos(\theta_t) + n_2 \cos(\theta_i)}\right]^2 \quad (4)$$

If the incident light is unpolarised (containing an equal mix of *s*- and *p*-polarizations), the reflection coefficient is:

$$R = (R_s + R_p)/2. \quad (5)$$

The transmission coefficient in each case is given by

$$T_s = 1 - R_s \quad (6)$$

$$T_p = 1 - R_p. \quad (7)$$

It should be noted however that application of the Fresnel equations to a system as complex as a modified interface requires a common but more advanced computation than the ones outlined above because of: a. multiple reflections within the multilayer stack, and b. the fact that that the optical constants are usually complex numbers that incorporate both the conventional refractive index and the absorptivity. To estimate the complex optical constants n_1 and n_2 effective medium theory is often used. This takes into account the optical constants of both the metal and the surrounding dielectric medium including the sample layer. The calculations of SEIRA enhancement of *p*-NBA[16] are in reasonable qualitative agreement with observation based on conventional multilayer Fresnel reflectivity calculations.

The effective medium models are used to compute an average complex refractive index for the surface layer based on the size and spacing of the metal spheroids and the absorption spectra of the absorbate molecules. Two models have been shown to be effective for this: the Maxwell-Garnett and the Bruggeman models.[16] The Maxwell-Garnett model works best when the packing density of the metal is small. However, when the metal particles are densely aggregated the Brugggeman effective medium theory is evidently more accurate.[16] These models may be succinctly expressed as:

Maxwell-Garnett model:

$$\epsilon_{MG} = \epsilon_h \ ((3 + 2F\alpha) / (3 - F\alpha)) \qquad (8)$$

Where ϵ_{MG} is the effective (space averaged) dielectric function

F is the packing density of the metal, defined as $F = d_{mass}/d_{opt.}$

d_{mass} is the mass thickness.

d_{opt} is the optical thickness.

α is the polarizability of the metal covered with adsorbed molecular layer.

ϵ_h is the dielectric constant of the surrounding medium.

Bruggeman model:

$$\epsilon_{BR} = \epsilon_h \ (3(1- F) + F\alpha)/ (3(1-F) - 2F\alpha) \quad (9)$$

Where ϵ_{BR} is the effective dielectric function.

F is the packing density of the metal, defined as $F= d_{mass}/d_{opt.}$

α is the polarizability of the metal covered with adsorbed molecular layer.

ϵ_h is the dielectric constant of the surrounding medium.

Effective medium approximations have not yet been attempted on the data collected in this study, but are planned for a subsequent analysis.

1.4 SEIRA Measurements

SEIRA measurements can be made using a variety of geometries including a) transmission mode,[30,33] b) surface reflection-absorption mode (RA),[11,34,35] and c) attenuated total reflection mode (ATR).[9,10,32,36,37] Diagrams of these optical geometries are illustrated in Figures 4a, b, and c respectively.

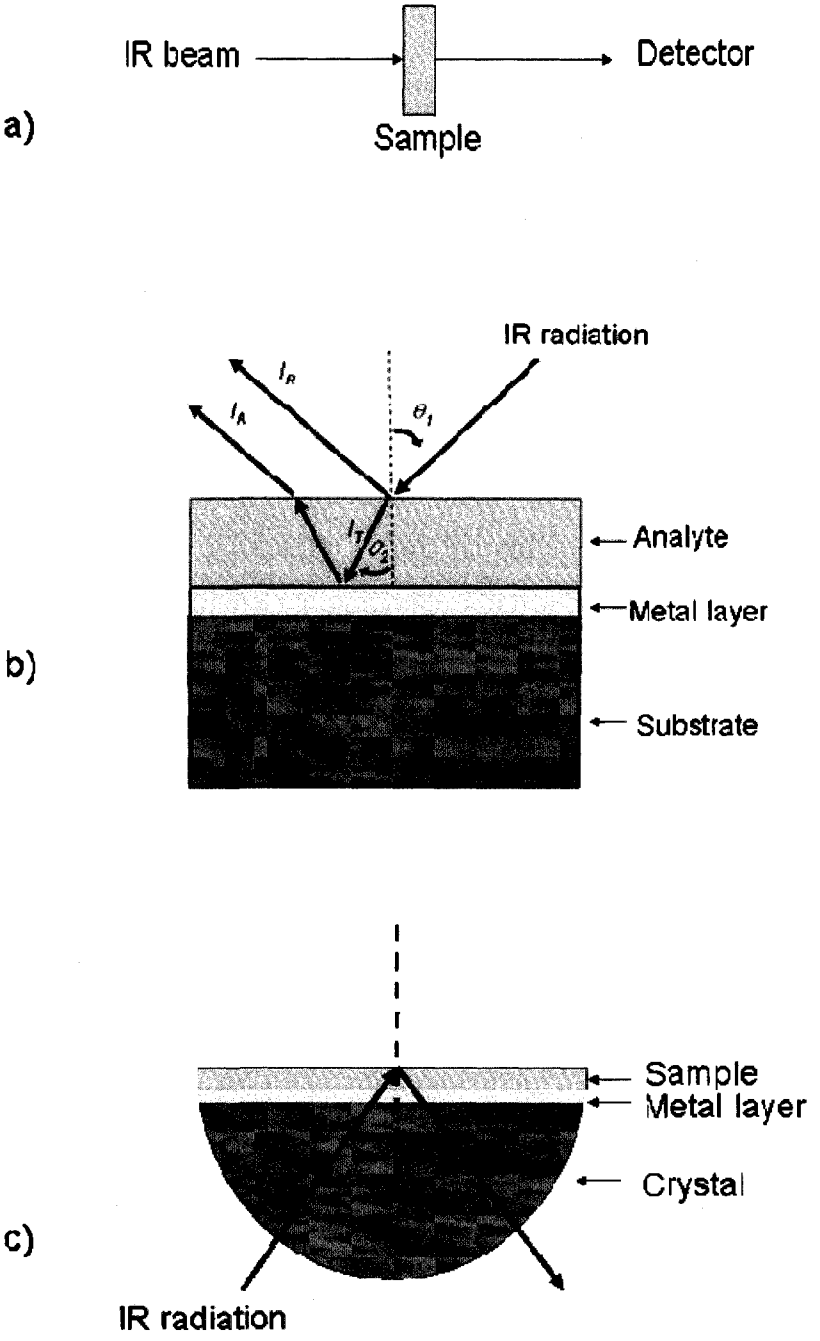

Figure 4. SEIRA set up a) transmission mode, b) surface reflection-absorption mode, and c) attenuated total reflection mode where θ_1 can be 60 to 80°.

1.4.1 Transmission mode

This method does not require additional instrumental accessories, as does the ATR mode or RA mode. A sample with the gold – analyte layer is simply placed into the sample compartment of an infrared spectrometer. This mode was used to collect data for the SEIRA experiments described in this thesis because a convenient optical sampling configuration is highly desirable in FTIR studies and otherwise can present a substantial barrier to the implementation of the method on a routine basis. Different sampling modes may in some cases provide a larger effective light path length (depending on the angle of incidence, e.g., surface reflection-absorption) or may be compatible with liquid samples (such as attenuated total reflection) so the method choice is clearly analyte dependent.

1.4.2 Surface Reflection-Absorption mode (RA)

This method measures the energy that is reflected off the surface of a sample. The incident beam penetrates through the analyte and then reflects off the metal back to the surface of the film. When the beam exits the thin film it has geometrically passed through the film twice and at an angle off of the surface normal. Therefore its absorbance intensities are typically 2 - 4 times those of the corresponding transmission mode experiment. Some of the energy that passes through the surface layer is absorbed by the sample and then reflects off of the substrate below the surface layer.

1.4.3 Attenuated Total Reflection mode (ATR)

This method operates by measuring the changes that occur in an internally reflected infrared beam when the beam comes into contact with a sample. An infrared beam is directed onto an optically dense material such as germanium or diamond with a

high refractive index at a certain angle which is greater than the critical incident angle of about 80°. The resulting internal reflectance creates an evanescent wave that goes beyond the surface of the crystal and penetrates into the sample to a depth of several hundred angstroms (which is held in contact with the crystal). ATR-SEIRA is a highly sensitive technique for both physiorbed and chemisorbed analytes with an enhancement which is often greater than twenty to thirty fold relative to the normal IR transmission technique.[5,20] This is due to the grazing incidence reflection absorption geometry which has an electric field perpendicular to the substrate surface, while the normal incidence transmission geometry has an electric field in the plane of the monolayer. This method was used during wet chemistry to analyze the nuclei and chemical plating on a coated Si surface.[32]

1.5 SEIRA Applications

As noted above, SEIRA is a very sensitive surface technique which in some cases yields over a hundred fold enhancement in the absorption signal of adsorbed analytes. It can be used for the detection of many adsorbate molecules located at the: metal-air, metal-liquid or metal-solid interfaces. In the opinion of the author, SEIRA as an analytical technique is still in its infancy and may find wide application in surface trace analysis where small concentrations must be detected with a percent accuracy greater than 90%.[16] In research settings SEIRA has also been used for biochemical sensors,[6,9] electrosoption,[32] and electrocatalysis.[37] It can also be used to determine the adsorption and desorption kinetics of multiple layers of material.[38] As an example, ATR-SEIRA is a

valuable tool for the investigation of the hydrogen bonding between silosane anchor carboxylic acid and the surrounding molecules.[39]

As was noted in the introduction, the working hypothesis that guided these experiments is that a thin Au coating will transform a simple silicon wafer support into a sensitive IR detector for ultrathin organic films, and specifically that a 5 nm Au coating will increase the IR absorbance signals of a molecular layers such as ones formed by *p*-NBA, the mercaptoalkyl acids, and silanes described above.

2. EXPERIMENTAL METHODS

2.1 Metal Deposition

The metal island films were deposited using either a Pelco SC-7 sputter system from Ted Pella, Inc. or a Denton Vacuum DV-515 vacuum evaporation system. The thickness and distribution of the gold coating is a function of several adjustable deposition parameters: chamber pressure, power setting, coating time and the target to table distance. These parameters were described below. A high purity gold sputter target was placed in the sputter disk of the Pelco SC-7 sputter system, which was located approximately 10 cm above the stage holding the Si substrate. Sputter deposition was done under argon at a pressure of 0.08 mb with a current of 40 mA. After 15 sec a 5 nm film was obtained. When using the DV-515 the evaporation took place under a pressure of 8×10^{-6} torr with a current at 32 - 35 A x 5 V on a small tungsten wire basket (Englhard-Clal B12b-040W). The film thickness was monitored and controlled by the thickness monitors, Pelco FTM-2 from Ted Pella, Inc. for sputtering and the TM-100 from Maxtek, Inc. for evaporated films. Reference FT-IR spectra were obtained promptly after gold deposition.

Prior to deposition of metal island films each of 1 x 2 inch polished Si substrates (p-type ~ 20 Ωcm) was rinsed three times with isopropanol and dried with N_2. The cleaning step is critical in order to remove any contamination due to air exposure prior to the deposition.[1-4,6,7,16,20]

2.2 Method of Annealing Au on a Si Substrate

In order to understand the effect of thermal annealing on the magnitude of the SEIRA effect, selected the Au sample were thermally annealed to enlarge the Au island features. We do not wish to imply that the conditions which were chosen in this experiment are optimal from the perspective of SEIRA enhancement – rather, guided by literature reports of successful SEIRA-active metal films we desired to make a preliminary judgment of the effect of thermal annealing on the SEIRA magnitude and to correlate this difference with the anticipated change in Au surface morphology. The annealing was done at 250°C in a Lindberg Blue-M furnace under a flow of N_2 at 30 cm^3/s for one hour. The Au sample was then cooled to room temperature before the deposition of 1 mM *p*-NBA in isopropanol. The annealed sample was then compared with a non-annealed sample in terms of SEIRA enhancement and correlating to structure via SEM and AFM images of grain morphology.

2.3 Method of Preparing Analyte Layers

p-NBA and mercaptoalkyl acids (3, 11, or 16) were used as test analytes for SEIRA technique refinements. *p*-NBA was dissolved in HPLC grade isopropanol (obtained from Aldrich) at a concentration of 0.001%. Droplets of 20 uL were pipetted onto the substrates (Si or Si|Au) yielding circular wetted areas of ~5 mm. Assuming a uniform distribution of pNBA across this layer corresponds to a 10 nm film thickness. Mercaptoalkyl acids were prepared as 1 mM solutions in isopropanol and substrates were

soaked in this solution for 10 minutes at room temperature and then removed from solution and dried in a nitrogen stream.

2.4 Method of Forming Secondary Layer of Silanes

Au coated Si samples were immersed in 1 mM isopropanol MUA solutions for 10 min at room temperature. The samples were then removed and dried under a stream of N_2.

Neat silanes were obtained from Gelest. Silane solutions in toluene were prepared at a concentration of 10 mM. Using a glove-box MUA treated Au samples were immersed in the silane solutions for 10 min. Samples were then rinsed five times with toluene and dried under a stream of N_2.

2.5 Instrumentation

2.5.1 Fourier Transform Infrared Spectroscopy

Vibrational spectra were recorded using a Nicolet 6700 FT-IR spectrometer. A DTSC TEC detector was used for these measurements. The frequency range was set from 4000 cm^{-1} to 400 cm^{-1}. The beam splitter was KBr. The gain number used during measurement was set at 2 with a mirror velocity of 0.6329 cm/s and an aperture setting of 100. The transmission mode was set with automatic atmospheric suppression. The number of scans was set at 64 with a resolution of 4 cm^{-1}. The final data was reported in the absorbance format.

2.5.2 Atomic Force Microscopy

The gold films were characterized with Atomic Force Microscopy (AFM) using a digital instruments dimension Veeco 5. The measurement was performed in tapping mode with an etched silicon cantilever. Images were collected in air with an ambient relative humidity in the range of 38 – 45 %. The AFM scan speed was set to 15 to 30 min per scan.

2.5.3 Scanning Electron Microscopy

Cross sections of the samples were evaluated by imaging on a Hitachi 4300 scanning electron microscope (SEM) with a thermal field emission source. Samples were cleaved and residual cleaving particles were removed by placing under a stream of N_2 for 30 sec. The accelerating voltage used during measurement was 2.5 kV and the working distance was 7 to 9 mm with an aperture of 6. The emission current was 8000 nA.

3. RESULTS and DISCUSSION

3.1 Substrate Deposition and Characterization

Among the many parameters that may affect the magnitude of SEIRA enhancement, the quality of the Au layer formed during metal deposition is perhaps the most important. Important film qualities may include the thickness of the metal layer, the size and shape of metal islands, and crystallographic aspects of the metal surface structure. Figures 5 a and b below show SEM images for gold metal films that were formed using the SC-7 evaporator and the DV-515 sputter systems respectively. These images show that the metal films consist of metal islands that are on average 40 - 60 nm in diameter. From the size and the number of the islands in a unit area, the average height of the gold islands was estimated to be about 1/4 of the diameter of the islands, which is approximately 10 nm to 12 nm.

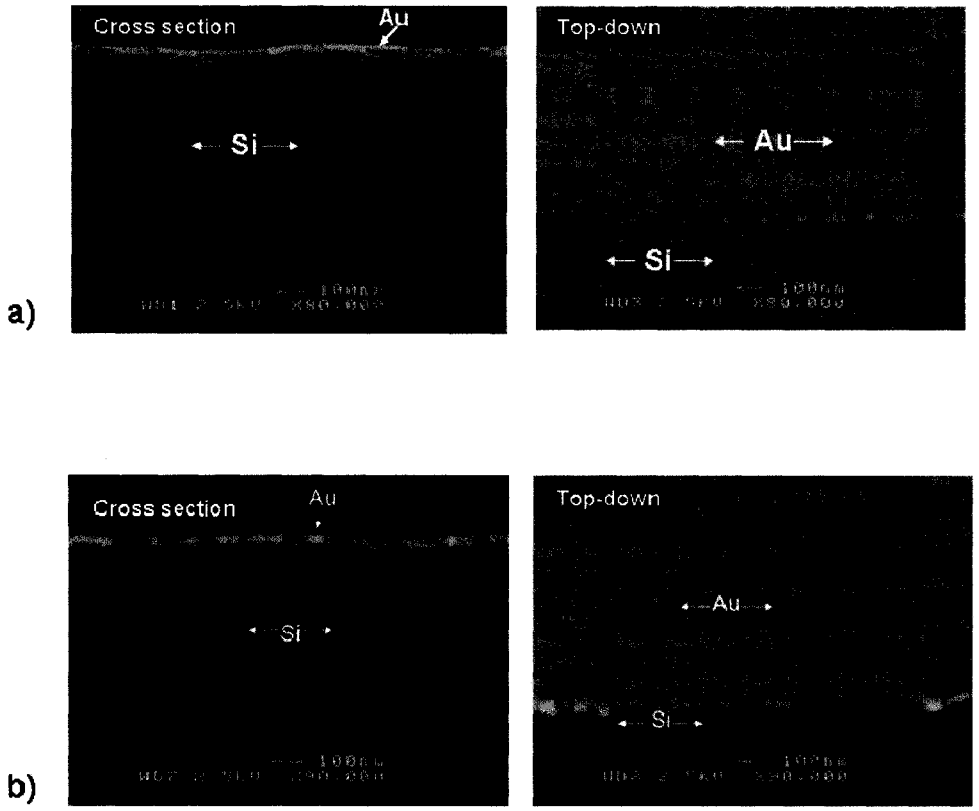

Figure 5. SEM images of gold layer on silicon substrate prepared with a) the DV-515 evaporator or b) the SC-7 sputter.

The 3D AFM images from Figure 6 show individual gold islands. The images also show that gold island growth is uniform across the silicon substrate on the micron scale and is highly corrugated with root mean square (RMS) roughness of approximately 20 Å for samples coated by thermal evaporation and 15 Å for sputtered coated samples. Literature reports of similar films showed strong surface enhancement.[22,23] Important guidelines for metal film preparation were derived from a range of reports in the literature. These indicated that the metal film surface roughness increases with increasing gold layer thickness up to 26 nm, but that beyond this limit the Au layer quickly becomes a continuous film and SEIRA enhancement is lost.[1,10,25]

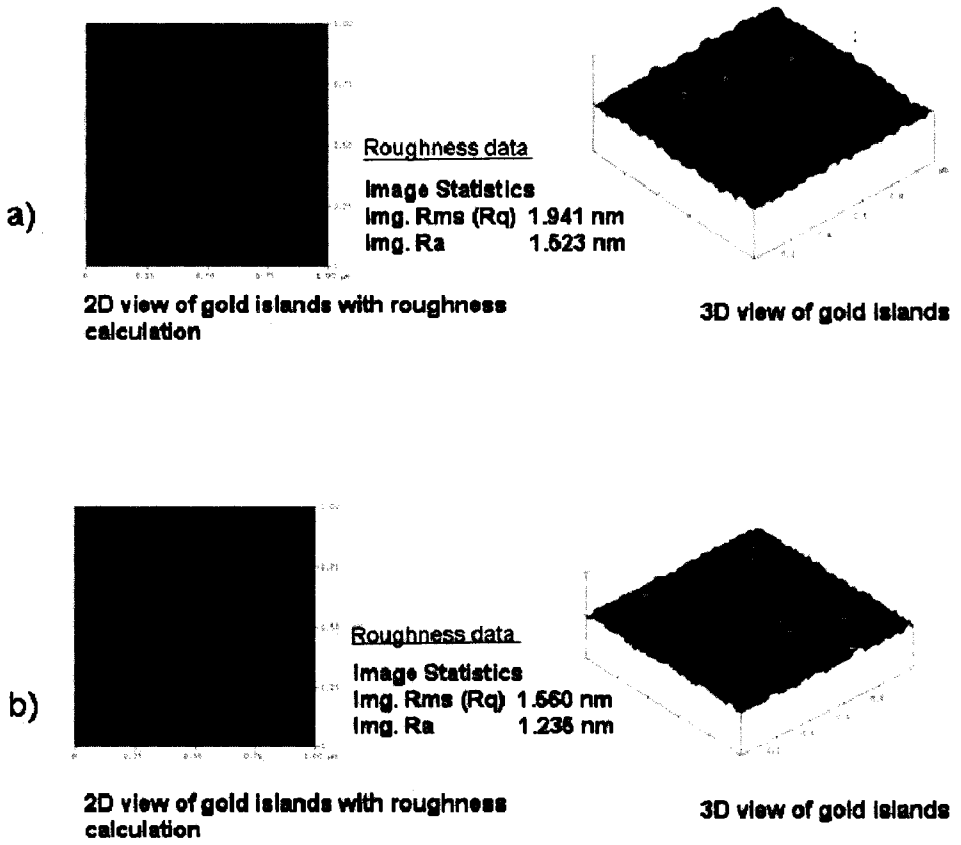

Figure 6. AFM images of gold on silicon substrate prepared with a) the DV-515 evaporator or b) the SC-7 sputter.

3.2 Comparison of SIERA to Conventional IR and the Effect of Annealing on Enhancement

Figure 7 contrasts transmission absorption FTIR spectra of *p*-NBA solutions and thin films prepared on Si, Si|Au, and thermally annealed Si|Au. Figure 7a shows the spectrum of a 1% solution of *p*-NBA in CCl_4. Figures 7b-d show spectra of approximately 1.0 nm *p*-NBA films prepared on the following substrates: b. polished Si, c.10 nm Au on polished Si, and d. polished Si with a 10 nm Au film that has been annealed for 1 hr at 250°C under N_2.

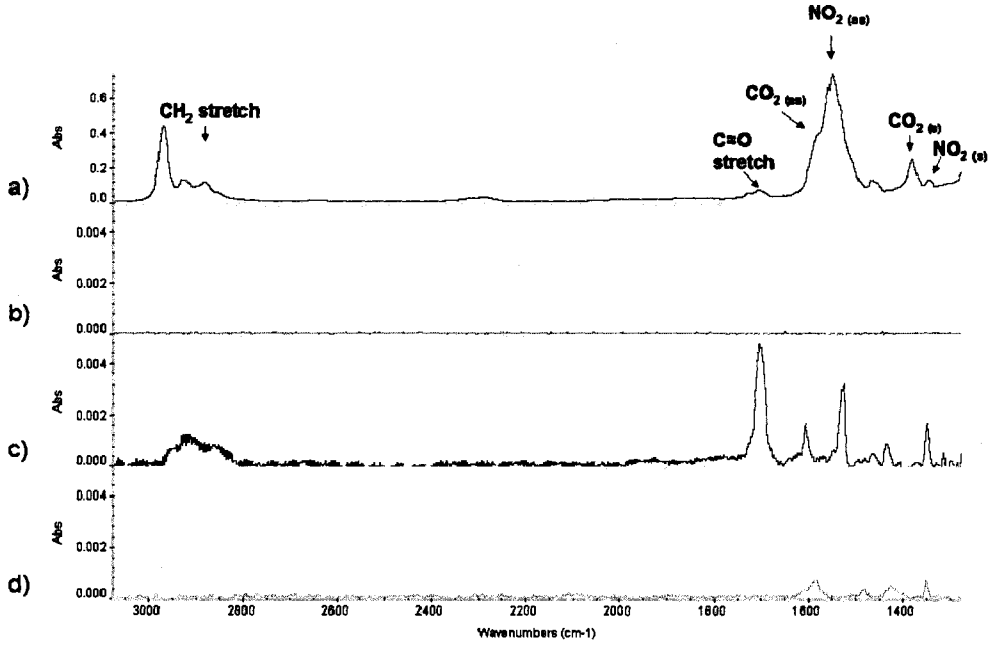

Figure 7. a) transmission IR absorbance spectrum of 1.0 % *p*-NBA in CCl_4 (50 μm path length), b) transmission IR absorbance of ~1.0 nm film of *p*-NBA on polished Si, c) SEIRA spectra of ~1.0 nm film of *p*-NBA on Au|Si, d) SEIRA spectrum of ~1.0 nm film of *p*-NBA on annealed Au|Si.

The band assignments for Figure 7 are based on a paper by Griffiths et al.[8] Clearly the presence of the Au layer is crucial to the detection of the organic film as no *p*-NBA signal was observed for identically prepared *p*-NBA films cast onto the Au-free substrate (a polished Si wafer surface). Band assignments are as summarized in the following Table 3:

Table 3. Band assignments for approximately a) 1.0 % *p*-NBA in CCl_4 (50 μm path length). 1.0 nm *p*-NBA films prepared on the following substrates: b) polished Si, c) 10 nm Au on polished Si, and d) polished Au film on polished Si that has been annealed for 1 hr at 250°C under N_2.

Freq. / cm^{-1}	Group Mode Assignment	Observed in Figure 7
2850 - 3000	CH_2 stretch	a and c
1750 - 1700	C=O stretch	a and c
1600	Anti-symmetric CO_2 stretch	a, c and d
1550	Anti-symmetric NO_2 stretch	a, c and d
1350	symmetric CO_2	a, c and d
1320	symmetric NO_2 stretch	a, c and d

The distribution of band intensities and widths differ dramatically between solution and solid ultrathin films on Au both as-deposited and annealed. Beginning with the comparison between solution and solid phase films (a and b), it is clear that the overall spectral changes are fairly complex. The CH resonances broaden substantially in the solid film, but in striking contrast, the NO and CO bands are substantially *narrowed.* Narrowing of course implies that either the film is relatively ordered or, inclusively, that the enhancement effect is selective within the inhomogeneous distribution of molecular orientations. The loss of rotational freedom in the p-NBA film may also contribute to this narrowing. If the band assignments are conserved, then one might venture to speculate that CO intensity is more enhanced than NO intensity, but: a. the surface structure is uncertain, and b. the possibility certainly exists that solution derived band assignments may be invalid for the collection of SEIRA bands observed in the 1300 - 1800 cm^{-1} region. While the exact assignments may be quite opaque in this setting, the simple fact that the strong enhancement is observed for *narrowed* bands is quite significant. The effect of Au annealing is also quite substantial. For example, the CH stretching band enhancement is attenuated below detection in the annealed-Au system, and the C=O, CO_2, and NO_2 bands again redistribute by a very large factor while retaining the very narrow bandwidths of the as-prepared Au system.

The CO_2 (as) and CO_2 (s) bands in Figure 7d are red shifted and enhanced after annealing as can be seen when compared to Figure 7c. The SEIRA enhancement of *p*-NBA observed in Figure 7c for the CH_2, C=O, NO_2 (as), and NO_2 (s) stretching disappears after annealing as shown in Figure 7d. With annealing, Au islands merge and

form large aggregates. The phenomenon of forming large Au islands is called grain growth. This occurs with the migration of grain boundaries, and subsequently leads to a loss of enhancement in SEIRA. The SEM images of Figure 8a illustrate the arrangement of approximately 6 - 8 nm Au islands deposited on Si which uniformly coat the substrate. Figure 8b shows the formation of large Au islands after annealing.

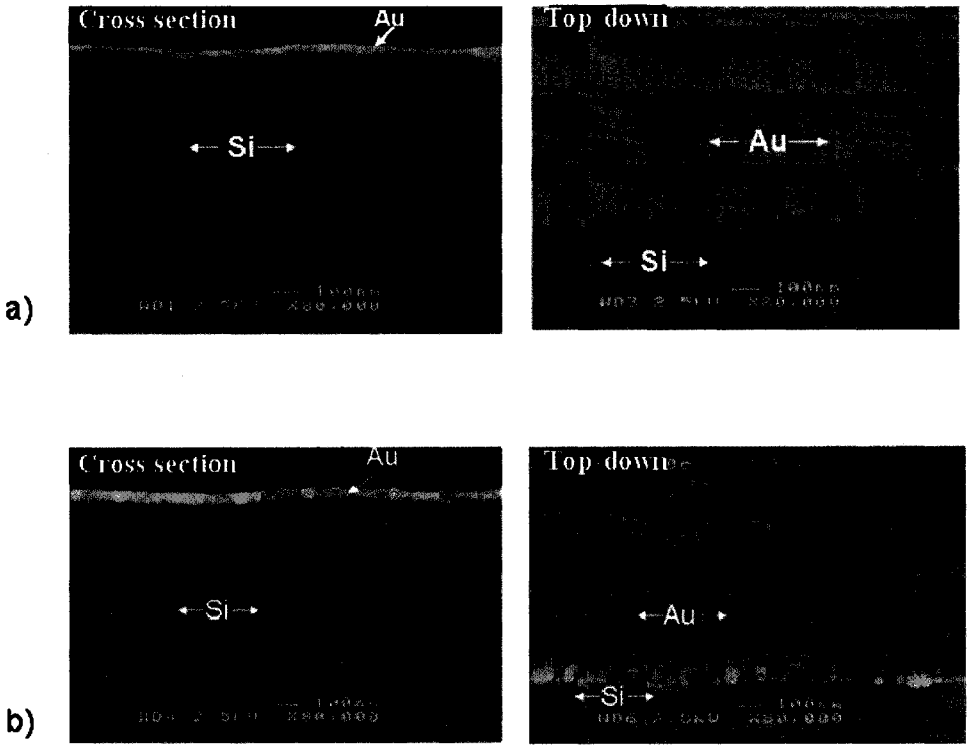

Figure 8. SEM images of the *p*-NBA on Au films a) before annealing and b) after annealing at 250°C for 1 hour under N_2.

3.3 Calculations for SIERA Enhancement

In order to place the observed band intensities in context, we performed a simple and approximate calculation of the apparent enhancement in absorption intensity. This calculation involved several steps. First, the approximate *p*-NBA film thicknesses were estimated as follows. The 20 μL droplet of 0.010 % ($^{w}/_{v}$) alcoholic *p*-NBA solution that was cast into a thin film was estimated to have dried in a uniform disc of 1.0 cm diameter (as was observed). The mass and approximate density of solid *p*-NBA was then used to compute the average approximate *p*-NBA film thicknesses, d_{PHYS} ~1.0 nm. Next, the free-solution extinction coefficients for selected bands were computed using a transmission spectrum of *p*-NBA in CCl_4 solution (1.0 % ($^{w}/_{v}$) × 50 μm). Referring back to the SEIRA spectra the *apparent* thickness of the solid films was calculated using Beer's law:

$$d_{APP} = A / (\epsilon_{CCl4} * c) \qquad (10)$$

Where d_{APP} is the apparent film thickness (cm)

A is the absorbance

ϵ_{CCl4} is the solution-phase molar absorptivity (L mol^{-1} cm^{-1}) and

c is the estimated concentration (mole L^{-1}) in the solid film

Table 4 illustrates the very large d_{APP} values observed for *p*-NBA films deposited on SEIRA substrates. This may be due to the SIERA surface selection rule effect on enhancement of the IR absorbance measured for the analyte on Au islands. SIERA enhancement is thus parameterized as the ratio of the apparent film thickness to the physical film thickness, d_{APP} / d_{act}.

In order to even more conservatively estimate this enhancement factor, a possible increase in signal due to an increase in surface area is also incorporated. Because the test substrates used were not smooth, but instead covered with Au islands, it might be argued that the increased surface area accounts for part or all of the increased signal that was observed. That is, for any given 2-D unit area of test substrate there should be a greater number of analyte molecules directly adsorbed to the surface than for the same unit area on an ideal smooth surface. To estimate such a contribution to the apparent enhancement was approximated based on a uniform hexagonal distribution of Au islands hemispheres Figure 9.

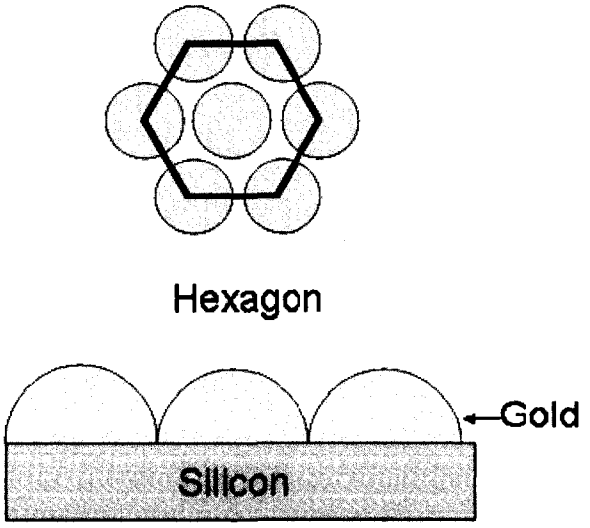

Figure 9. An approximate surface area calculation for hexagonal array of Au hemispheres.

A hexagonal area unit contains a total of seven atoms - six peripheral and one central. Each of the six peripheral atoms contributes 1/3 of its surface to the hexagonal cell while the central atom contributes all of its area. The surface area of each island hemisphere is $4\pi r^2/2$ where r is the hemisphere radius. Thus the total Au surface area in a given hexagonal area unit is $A_{Au} = 6 \cdot (\frac{1}{3} \cdot \frac{4 \cdot \pi \cdot r^2}{2}) = 4 \cdot \pi \cdot r^2$. Dividing this by the area of the corresponding flat hexagon, $A_{Geom} = \frac{3\sqrt{3}}{2} r^2$, yields an increase in surface area by a factor of $\frac{A_{Au}}{A_{Geom}} = \frac{4\pi r^2}{\frac{3\sqrt{3}}{2} r^2} \approx 1.8$. Even allowing for this modest factor the enhancement values are still as large as ~1000 See Table 4.

Table 4. SEIRA enhancement calculation for *p*-NBA

Molecule	Band Assignment / Frequency	1% p-NBA in solution		p-NBA deposited on Au/ Si substrate		Enhancement Calculation	
		A	ε_{ma} (L/mole cm)	A	$d_{APP} = A/(\varepsilon_{ma}*c)$	d_{APP} / d_{PHYS}	$d_{APP}/(1.804* d_{PHYS})$
p-NBA	CH stretch 3100 - 2800 cm^{-1}	0.48	890	0.0015	150	150	**130**
	CO_2 asymmetric 1500 - 1450 cm^{-1}	0.34	630	0.0015	220	220	**190**
	NO_2 asymmetric 1500 - 1450 cm^{-1}	0.7	1300	0.003	210	210	**180**
	CO_2 symmetric 1350 - 1300 cm^{-1}	0.24	440	0.0011	230	230	**200**
	NO_2 symmetric 1400 - 1350 cm^{-1}	0.12	220	0.0013	540	540	**460**
	C=O 1750 - 1700 cm^{-1}	0.17	310	0.0038	1120	1120	**950**

3.4 SEIRA Results for Molecular Monolayers

In these studies monolayers of selected molecules were prepared on Si|Au substrates to evaluate their SEIRA absorbance. A subsequent section will describe experiments wherein one of these molecules, mercaptoundecanoic acid, was used as an anchor layer for secondary molecular overlayers and SEIRA intensities for these systems will be evaluated as well. The analytes used for monolayer studies are 3-mercaptopropinoic acid (MPA), 11-mercaptoundecanoic acid (MUA), and 16-mercaptohexadecanoic acid (MHA). In most Figures the absorbance spectrum of a drop-cast film of MUA, on polished Si anticipated to be roughly 1.0 nm thick is included for comparison.

Thin layers of Au (approximately 7nm) were prepared on a Si substrates and their transmission spectra recorded as reference. Mercaptoalkanoic acids were then chemisorbed to the Au surface. These substrates were used to measure SEIRA enhancement – see Figures 10-12 below. The band assignments for these molecules are based on seminal work by Allara and others.[40-44] Clearly the presence of the Au layer is crucial to the detection of the organic film since there was no signal observed on the same molecule (MUA) deposited on polished Si. Band assignments are as summarized in Table 5:

Table 5. Band assignments for analytes adsorbed onto Au surface where: a)is16-mercaptohexadecanonic acid (~ 1.4 nm), b) is 11-mercaptoundencanoic acid(~1.0 nm), c) is 3-mercaptopropionic acid (~0.4 nm), and d) is 11-mercaptoundencanoic acid deposited on bare Si (~10 nm) for comparison.

Freq. / cm^{-1}	Group Mode Assignment	Observed in Figure 14, 15, 16
2850 - 3000	CH_2 stretch	a, b
1750 - 1700	C=O stretch	a, b, and c
1460 - 1400	carboxylate symmetric stretch + CH_2 scissor	a, b, and c
1350 - 1150	CH_2 rock / wag	a, b, and c
750 - 700	CH_2 bend	a, b, and c

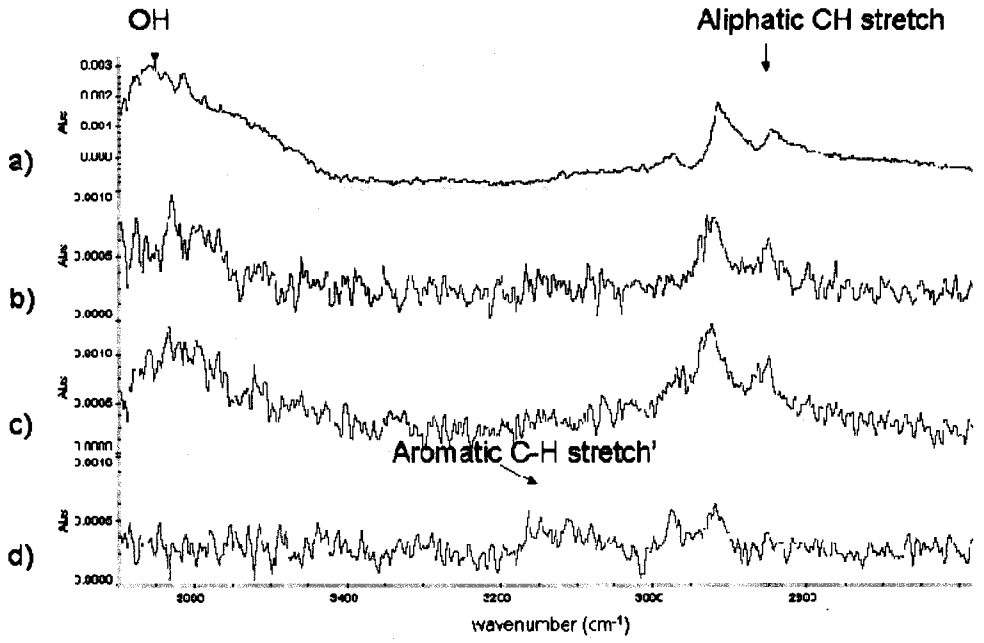

Figure 10. High-frequency SEIRA spectra in the 2700 - 3500 cm^{-1} region. Analytes adsorbed onto Au surface where: a) is 16-mercaptohexadecanonic acid (~ 1.4 nm), b) is 11-mercaptoundencanoic acid (~1.0 nm), c) is 3-mercaptopropionic acid (~0.4 nm), and d) is 11-mercaptoundencanoic acid deposited on bare Si (~10 nm) for comparison.

Figure 10a-c shows the C-H stretching region for the three molecules. The symmetric and antisymmetic stretches are observed at 2850 and 2926 cm^{-1} respectively. These bands are both strong and informative as their frequencies are known to be sensitive to the state of crystallinity of the alkyl chain, so a comparison with literature values is relevant and yields the following qualitative conclusion. The limited resolution of these spectra prohibits detailed analysis, but those values observed are within the range observed for liquid alkanes 2924 cm^{-1} and crystals 2855 cm^{-1} and are consistent with literature values for n-alkanethiols on continuous Au films.[40-45] In Figure 10d, MPA does not exhibit a measurable signal for the C-H stretch. This is due in part to the short alkyl chain - there are only four alkyl hydrogens on MPA compared to twenty on MUA and thirty on MHA. But if all methylene hydogens absorb equivalently, then a measurable absorbance peak ($\frac{4}{20} \cdot 0.002 \approx 0.0004$) might arguably be resolved above the local noise envelope (0.0002). This suggests that either these particular modes oscillate more nearly parallel to the local surface plane in MPA or perhaps that so near the surface there may be a point of relatively low enhancement. On the other hand, since CH wagging and bending modes observed for all three Figure 11, the former orientation effect would seem more likely.

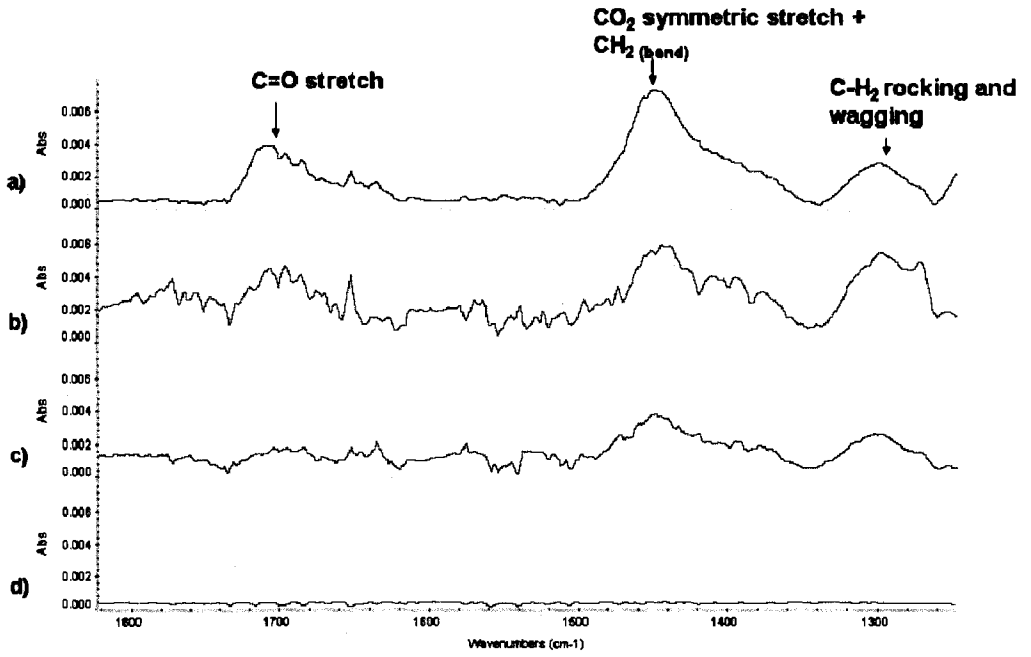

Figure 11. Mid-frequency SEIRA spectra in the 1300 - 1800 cm^{-1} region. Analytes adsorbed onto Au surface where: a) is 16-mercaptohexadecanonic acid (~ 1.4 nm), b) is 11-mercaptoundencanoic acid (~1.0 nm), c) is 3-mercaptopropionic acid (~0.4 nm), and d) is 11-mercaptoundencanoic acid deposited on bare Si (~10 nm) for comparison.

In Figure 11 one observes a prominent band in the region 1700 – 1750 cm^{-1} range, assigned to the CO stretching mode of the carboxylate.[40-44] This band is relatively strong for MHA, weak for MUA and barely evident for MPA. Since the coverage of these molecules is expected to be quite similar the relative intensity differences again deserve some comment. Since the atomic motions associated with this mode are predominantly along a single C=O bond axis, rotation of the carbonyl group can change the surface projection of the corresponding transition dipole moment very substantially, and correspondingly impact its absorption strength. So, weakness in the MPA case may be due to a different carboxylate headgroup orientation. This is supported by an ATR-SEIRA study of MPA adsorption from ethanol and chloroform. In this study, surface hydrogen bonding between adjacent MPA molecules is implied to pull the C=O bond into an orientation nearly parallel to the local Au surface, which might account for the diminished C=O intensity in MPA relative to MUA/MHA films.[36] This is also consistent with the ~1710 cm^{-1} frequency observed in this study – free C=O is observed at ~1750 cm^{-1}. However, distance dependence to the SEIRA effect may also underpin this difference diminution in intensity.

Literature spectra for MUA monolayers on smooth gold (obtained by grazing angle external reflection) show similar band frequencies to those that we observed for MPA, MUA, and MHA.[40-44] The band observed between 1400 – 1460 cm^{-1} is assigned to a mixture of CH_2 scissor deformation and the symmetric CO_2 stretch absorption, the band at 1300 - 1380 cm^{-1} is assigned to a mixture of CH_2 rocking and wagging motions and the 700 - 800 cm^{-1} bands are assigned to CH_2 bending modes.

Band intensities are summarized in Table 6, which also shows the approximate calculated enhancement for MHA, MUA, MPA modes on the Au layer. The calculated enhancement values for these molecules were in the range of 180 to 300. The band intensities that we observed were quite similar to those observed by Imae and colleagues (0.0015 - 0.0027) but our band strengths consistently increased with decreasing frequency, and at 1150 - 1350 cm^{-1} exceed those of the Imae study by about a factor of four. This is further reflected in the large enhancement values that we compute for bands in the 1150 - 1350 cm^{-1} range (200 - 500). Our results also trend oppositely in to the unenhanced external reflection measurements of Nuzzo et al.[2] and Corn et al.,[40,41] in which studies very smooth, continuous, and relatively thick Au films approximating bulk Au surfaces were employed. This trend clearly implies a frequency dependence of the magnitude of the SEIRA enhancement that increases at lower infrared frequencies – possibly due to a stronger electromagnetic resonance at the lower frequency.

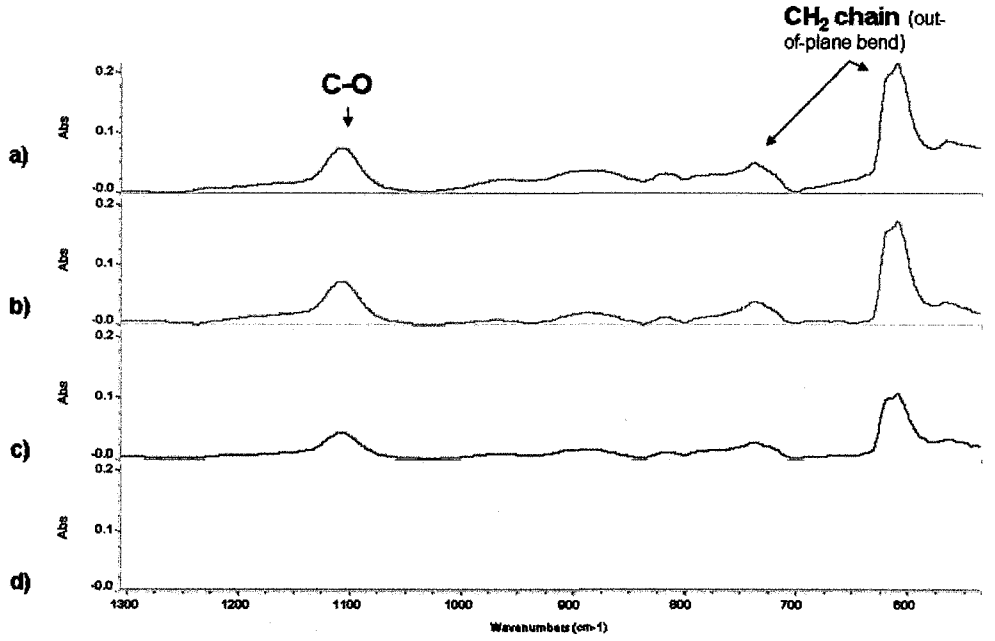

Figure 12. Low-frequency SEIRA spectra in the 650 - 1200 cm^{-1} region. Analytes adsorbed onto Au surface where: a) is 16-mercaptohexadecanonic acid (~ 1.4 nm), b) is 11-mercaptoundencanoic acid (~1.0 nm), c) is 3-mercaptopropionic acid (~0.4 nm), and d) is 11-mercaptoundencanoic acid deposited on bare Si (~10 nm) for comparison.

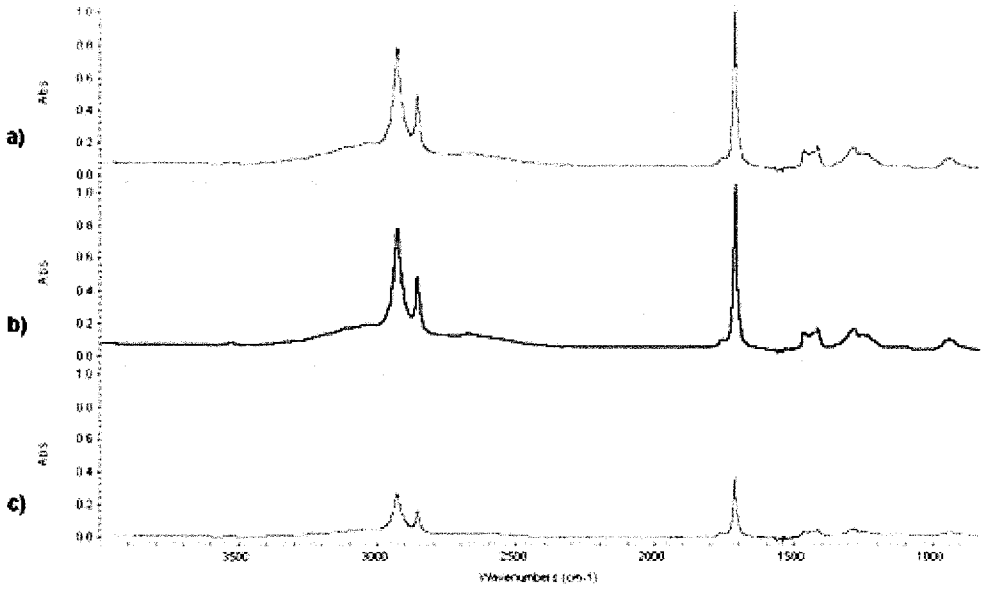

Figure 13. a) 1% of 16-mercaptohexadecanonic acid, b) 11-mercaptoundencanoic acid, and c) 3-mercaptopropionic acid (~0.4 nm) in CCl_4 collected using a 50 mm pathlength NaCl cell.

Table 6. SEIRA enhancement calculations for MUA, MHA, and MPA on Au surface.

Molecule	Band Assignment / Frequency	1% solution		1mM solution deposited on Au/ Si substrate		Enhancement Calculation	
		A	ε_{ma} (L/mole cm)	A	$d_{APP} = A/(\varepsilon_{ma} * c)$	d_{APP} / d_{PHYS}	$d_{APP}/(1.804 * d_{PHYS})$
MUA	CH 3100 - 2800 cm^{-1}	0.875	634	0.0015	90	50	**26**
	C=O 1750 - 1700 cm^{-1}	0.956	693	0.0035	180	70	**339**
	COOH + CH_2 scissor 1440 - 1400 cm^{-1}	0.200	145	0.0035	880	240	**133**
	CH_2 rock / wag 1350 - 1150 cm^{-1}	0.156	113	0.0061	1960	420	**234**
MHA	CH stretch 3100 - 2800 cm^{-1}	0.895	475	0.0025	140	25	**14**
	C=O stretch 1750 - 1700 cm^{-1}	0.998	529	0.0038	190	30	**16**
	COOH + CH_2 scissor 1440 - 1400cm^{-1}	0.600	318	0.0065	540	70	**39**
	CH_2 rock / wag 1350 - 1150 cm^{-1}	0.166	88	0.0036	1080	600	**335**
MPA	CH 3100 - 2800 cm^{-1}	0.258	698	-	-	-	**-**
	C=O 1750 - 1700cm^{-1}	0.357	966	0.002	280	210	**120**
	COOH + CH_2 scissor 1440 - 1400cm^{-1}	0.038	103	0.003	3850	1710	**950**
	CH_2 rock / wag 1350 - 1150cm^{-1}	0.036	97	0.002	2770	840	**490**

3.5 SEIRA Analysis of Si|Au|MUA|Silane Multilayers

As mentioned in the previous section, mercaptoalkyl acids are interesting not only as analytes, but also as linkers for a second generation of analytes which by themselves do not bind to Au. In our study, MUA was used as the linker and a variety of silane based molecular layers were reacted with it. This serves as a test of both the silyl reactivity and the SEIRA enhancement for this second molecular layer that is slightly removed from the Au surface. The following compounds were reacted with pre-formed Si|Au|MUA layers and then rinsed and analyzed: N-(2-aminoethyl) 3-aminopropyl trimethoxysialne (AEAP-TM), vinyldimethyl chlorosilane (VDM-Cl), and phenyldimethylsilyl chloride (PhDM-Cl). Figure 14 shows the mechanism of silylester formation which links the "second generation" silane layer at the Au|MUA surface.

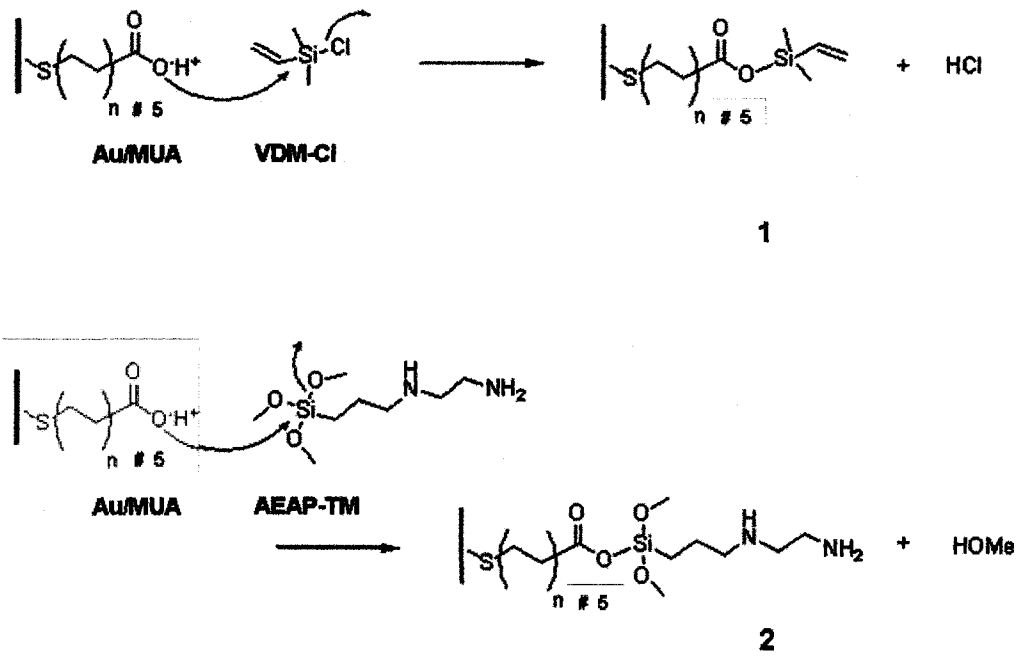

Figure 14. Mechanism of MUA-analyte linkage through silylester formation.

SEIRA spectra are presented in Figures 15, 16, and 17 in the high mid and low frequency ranges respectively, and for a representative MUA layer (a), AEAP-TM (b), VDM-Cl (c), and PhDM-Cl (d) layers respectively. It is important to note at the outset that the SEIRA spectra below use their respective Si|Au|MUA as blanks so the net absorbance observed is due exclusively to either: a. the silyl overlayer, or b. any contributions from structural changes (i.e., changes to the C=O or CO_2 resonances) that occur due to silylester formation or c. any changes in the magnitude of the SEIRA effect induced by the formation of the relatively high refractive index second generation layer.

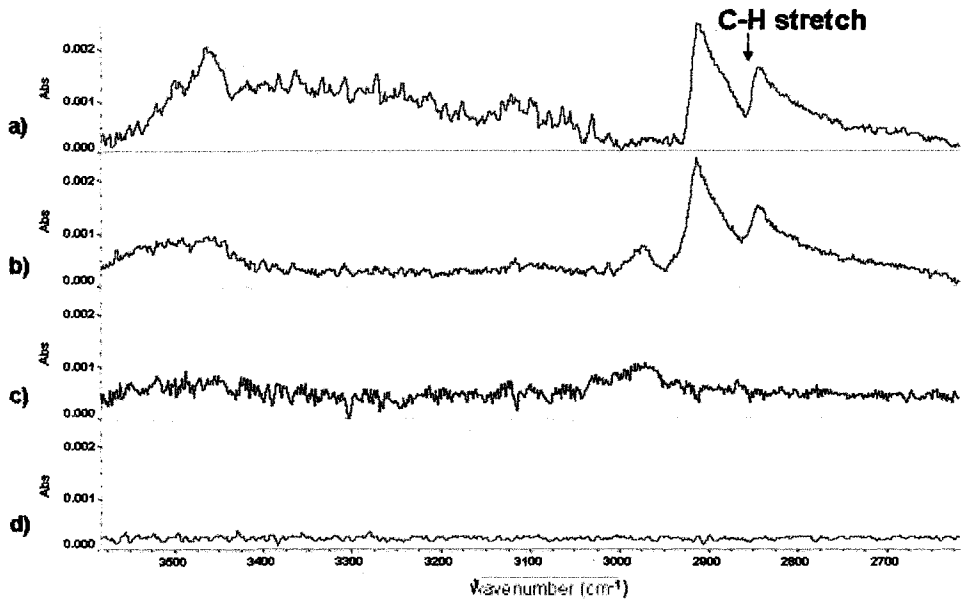

Figure 15. High-frequency SEIRA spectra in the 2500 - 3900 cm^{-1} region of analytes deposited on MUA/ Au/ Si substrate treated with a) nothing, b) AEAP-TM, c) VDM-Cl, and d) PhDM-Cl.

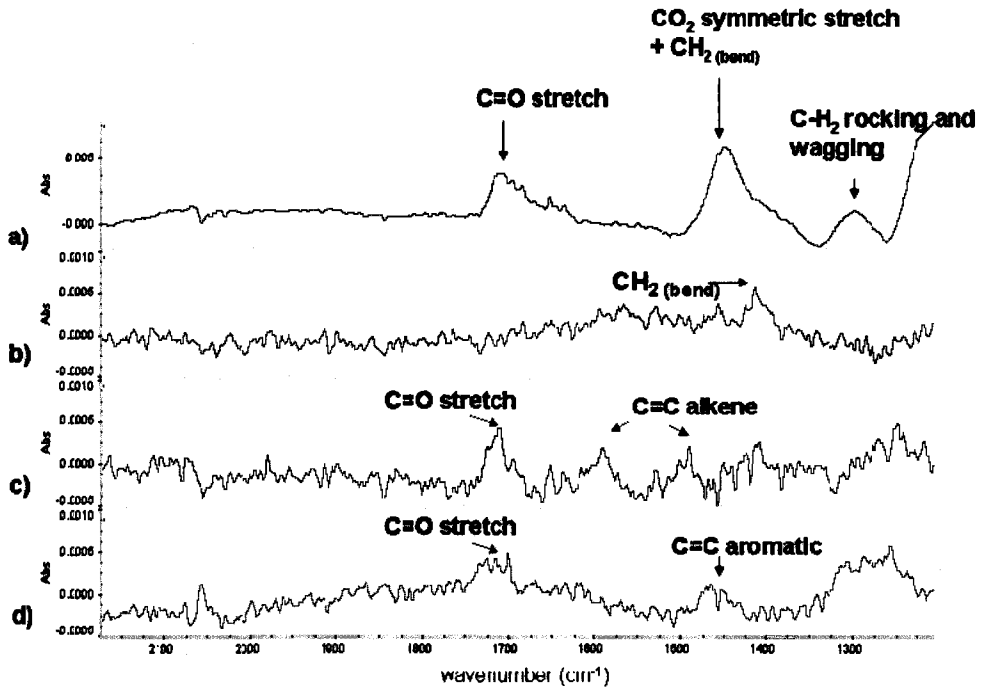

Figure 16. Mid-frequency SEIRA spectra in the 1200 - 2100 cm^{-1} region of analytes deposited on MUA/ Si substrate treated with a) nothing, b) AEAP-TM, c) VDM-Cl, and d) PhDM-Cl.

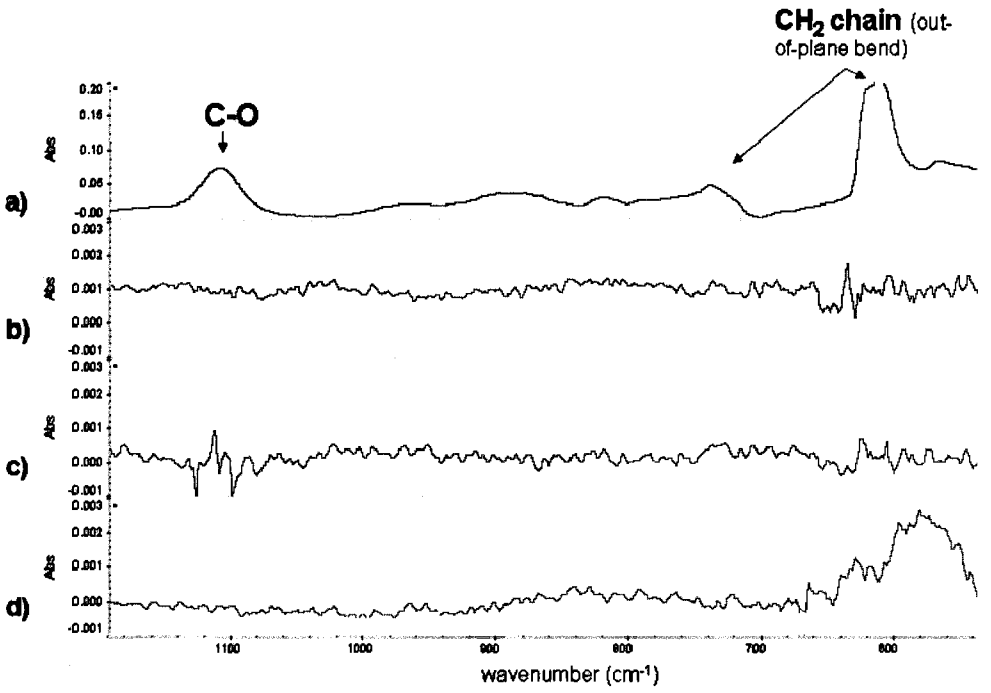

Figure 17. Low-frequency SEIRA spectra in the 500 - 1200 cm^{-1} region of analytes deposited on MUA/ Si substrate treated with a) nothing, b) AEAP-TM, c) VDM-Cl, and d) PhDM-Cl.

Figures 15-17a show the unmodified MUA layer referenced to Si|Au, and are similar to the above MUA spectra (Figure 10b) showing strong CH stretching modes in the 3000 cm^{-1} region in addition to a broad OH band near 3700cm^{-1}. The AEAP-TM results in Figures 15-17b show only weak C-H modes and no evidence of an NH band was observed in the 3500 - 3100 cm^{-1} range. The amplitudes of the C-H bands are roughly ¼ that of the original MUA layer (Figure 15a). Given the relative abundances of the C-H chromophore on MUA (20 per molecule) and AEAP-TM (16 per molecule) this is not unreasonable. It is also likely that the putative silane monolayer may be substantially lower density than the alkanethiol SAM one given the steric bulk of the trimethoxysilyl group at the point of attachment. Lastly, one might also anticipate a small SEIRA effect for this second layer given its distance from the Au surface. This being said, it is still possible that very little reaction may have taken place. The absence of NH resonance may simply be a signal-to-noise issue as there are only three NH bonds per molecule, but no band was seen. No band attributable to Si-O-CH_3 was observed, nor was an Si-O-Si resonance which might form if adjacent silanes cross-linked. These bands would be expected near 1600 cm^{-1} (see solution phase spectra in Figure 18). Lastly, if the silyl ester had formed with the carboxylic acid it might also be expected to replace OH band intensity with a band characteristic of the silyl ester but this was not observed – rather a very slight intensification of the OH region was observed.

The two chlorosilanes VDM-Cl and PHDM-Cl had largely similar results - i.e., CH resonances but no loss of OH but with some additional bands that were consistent with reactivity. For example, the PHDM-Cl spectra in 15, 16, and 17d show evidence of

aromatic CH, aromatic C=C, and CH bending modes characteristic of the phenyl group. Interestingly, both VDM-Cl and PHDM-Cl spectra present a weak band in the C=O stretching region in Figures 16c and d, but AEAP-TM does not. The presence of this band can only be attributed to an intensification of the existing MUA C=O stretching mode without substantial frequency shift as it does not have a derivative line shape. The putative VDM-Cl layer presents (16c) a bands characteristic of the vinyl group.

An alternate hypothesis for the lack of Si-O-CH_3 bands in Figure 17b (or possibly elsewhere) is the loss of Au islands due to silanes undercutting the Au islands. But since the blank was Si|Au|MUA, in this case one would expect strong negative absorbance features corresponding to Au and MUA and these were not observed.

Of the three silanes examined, the weakest case for derivatization is in the case of the AEAP-TM. One might rationalize this based on the relatively low reactivity of the methoxy silane since methoxy is among the less reactive leaving groups in Si based on S_N2 reactions*.[17] Aside from the expected bands near 1600 cm^{-1} for Si-OCH_3, this molecule lacks distinctive chromophores, leaving this case somewhat ambiguous. Given this result enhancement calculations for this molecule are omitted. AFM images of the original Au, Au|MUA and Au|MUA|silane layers are shown in Figure 19.

* The reactivity order for these silanes is chloride > amino > methoxy.

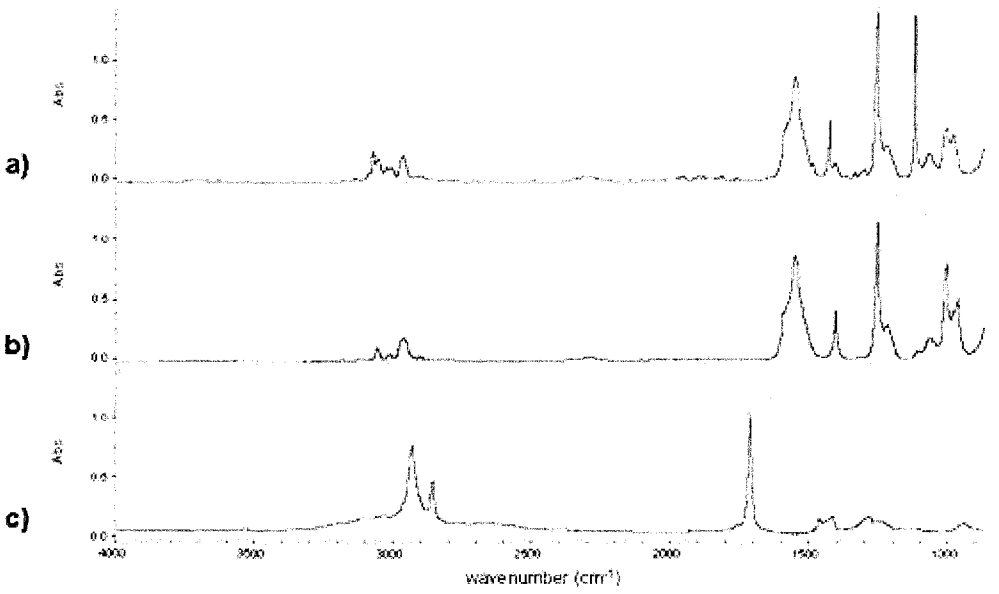

Figure 18. 1% analytes in CCl_4 solution where: a) is PhDM-Cl, b) is VDM-Cl, and c) is MUA collected through a NaCl window.

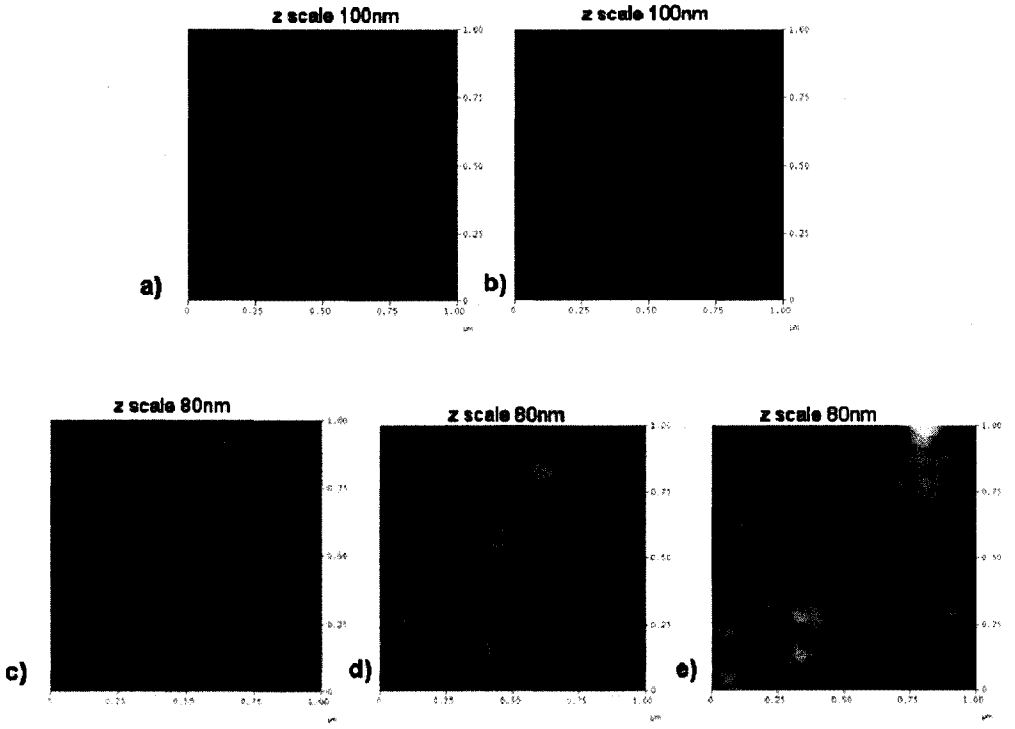

Figure 19. One by one micron AFM images of a) Au, b) Au|MUA, c) Au|MUA|AEAP-TM, d) Au|MUA|VDM-Cl, and e) Au|MUA|PhDM-Cl

Little difference was anticipated between the Au and Au|MUA surfaces since MUA is only expected to be 1.0nm thick. Indeed, only slight differences in texture were observed between the Au|MUA and the assumed Au|MUA|AEAP-TM layer from - see Figure 19b and Figure 19c. The chlorosilane layers were clearly different in Figure 19d and 19e. Images were dominated by nodular structures that were much wider (100 nm) than the original Au islands (20 nm), and somewhat taller (50 nm) than the original Au islands (20 nm). If these data are truly representative of the sufaces then it would seem likely that the chlorosilanes may have undergone a nucleated polymerization reaction of some sort.

The true physical dimension of the monolayer, $d_{PHYS} \sim 0.5$ nm, was estimated using CambridgeSoft Chem3D and using a simple geometry optimization employing CS MOPAC Pro at the AM1 level that had little impact on the result. With this approximation to d_{PHYS}, the band intensities were analyzed and an apparent enhancement computed. The solution-phase spectra shown in Figure 17 were used to derive extinction coefficients for the modes listed and the corresponding bands in the surface spectra were used as above to compute the approximate relative enhancements. Table 7 shows the results for the chlorosilanes and according to this the CH and C=C modes appear to be strongly enhanced. Of course, these enhancements are in inverse proportion to the layer thickness d_{PHYS} so these values must be considered upper estimates.

Table 7. Enhancement comparison for MUA/VDM-silyl and PhDM-silyl monolayers.

Molecule	Band Assignment / Frequency	1% solution of silane: A	1% solution of silane: ε_{ma} (L/mole cm)	Silane Deposited onto Au|MUA: A	Silane Deposited onto Au|MUA: $d_{APP} = A/(\varepsilon_{ma}*c)$	Calculated Apparent Enhancement: d_{APP} / d_{PHYS}	Calculated Apparent Enhancement: $d_{APP}/(1.804* d_{PHYS})$
VDM-Cl $d_{PHYS} \sim 0.5$ nm	CH stretch 3100 - 2800 cm^{-1}	0.277	400	0.0015	270	600	**330**
	C=C alkene 1600 - 1400 cm^{-1}	0.900	1170	0.00025	16	40	**20**
	CH_2 rock / wag 1350 - 1150 cm^{-1}	1.000	1460	0.0005	25	60	**30**
PhDM-Cl $d_{PHYS} \sim 0.85$ nm	Aliphatic CH stretch 3100 - 2800 cm^{-1}	0.168	200	0.0006	185	220	**120**
	Aromatic CH stretch 3100 - 2800 cm^{-1}	0.237	290	0.0004	86	100	**60**
	CH_2 rock / wag 1350 - 1150 cm^{-1}	1.510	1810	0.0005	17	10	**5 (±2)**
	C=C out of plane bend 800 - 700 cm^{-1}	3.500	4230	0.002	29	10	**6 (±2)**

4. CONCLUSIONS

Remarkably strong SIERA enhancements were observed in transmission FTIR experiments using ~7 to 8 nm sputtered and evaporated Au island films on polished Si. Thermal annealing of the Au was found to both increase the island sizes (according to AFM and SEM images) and to strongly decrease the SEIRA magnitude. Both physisorbed *p*-NBA and chemisorbed mercaptoalkyl acids exhibited enhancements as large as 100 to 300 fold and for a broad range of modes (e.g., CH_2 stretch, C=O stretch, anti-symmetric CO_2 stretch, or symmetric CO_2 stretches). Absorbance signals for a secondary silane layers bound to mercaptoundecanoic acid were much weaker, but assuming monomolecular silane layers were still strongly enhanced for selected modes ranging from 5 to 100 fold. This diminution at the secondary layer indicates that: a. the enhancement phenomenon may attenuate quickly as a function of distance from the surface, and therefore that b. the protocol may not be as sensitive a tool for secondarily bound layers. However, transmission mode SEIRA using polished Si substrates with thin Au layer thickness ranging from 20 to 80 Angstroms may prove a powerful method for trace detection of surface adsorbing species as it yields strong signals for as little as 1 nm of adsorbed material corresponding to submonolayers detection limits. Interesting future work may include the development of new chemistries that enable surface linkage of either a broader range of analytes, or in contrast, a more selective set of surface linkers that target specific analytes. This for example would be especially useful as a forensic chemistry sensor where the detection of a given molecule of interest (e.g., illicit drugs or explosives and their precursors) may be present at low concentrations in a complex

mixture of compounds. At such a point it would begin to be possible to define the concentration detection limits for this type of sensor.

REFERENCES

1. Hartstein, A.; Kirtley, J.R.; Tsang, J.C. *Phys. Rev. Lett.* **1980**, *45*, 201-204.
2. Noda, H.; Wan, L.; Osawa, M. *Phys. Chem. Chem. Phys.* **2001**, *3*, 3336-3342.
3. Zhang, J.; Zhao, J.; He, H. X.; Li, H.L.; Liu, Z.F. *Thin Solid Films* **1998**, *327-329*, 287-290.
4. Kamata, T.; Kato, A.; Umemura, J.; Takenaka, T. *Langmuir* **1987**, *3*, 1150-1154.
5. Merklin, G.; Griffiths, R. *Langmuir* **1997**, *13*, 6159-6163.
6. Brown, C. W.; Li, Y.; Seelenbinder, J. A.; Pivarmik, P.; Rand, A. G.; Letcher, S. V.; Gregory, O. J.; Platek, M.J. *Anal. Chem.* **1998**, *70*, 2991-2996.
7. Domingo, C.; Garcia-Ramos, J.V.; Sanchez-Cortes, S.; Aznarez, J.A. *J. Mol. Struct.* **2003**, *661*, 419-427.
8. Merklin, G.; Griffiths, P. R. *J. Phys. Chem. B* **1997**, *101*, 5810-5813.
9. Smith, B. M.; Franzen, S. *Anal. Chem.* **2002**, *74*, 4076-4080.
10. Sudo, E.; Esaki, Y.; Sugiura, M.; Murase, A. *Appl. Spectrosc.* **2007**, *61*, 269-275.
11. Brewer, S. H.; Anthireya, S. J.; Lappi, S. E.; Drapcho, D. L; Franzen, S. *Langmuir* **2002**, *18*, 4460-4464.
12. Zangeneh, M; Terrill, R. *Appl. Spectrosc.* **2004**, *58*, 10-17.
13. Badilescu, S.; Ashrit, P.V; Truong, V.; Badilescu, I. *Appl. Spectrosc.* **1989**, *43*, 549-552.
14. Alvarez, M. M.; Khoury, J.T.; Schaff, G. T.; Shafigullin, M.N.; Vezmar, I.; Whetten, R.L. *J. Phys. Chem. B* **1997**, *101*, 3706-3712.

15. Ung, T.; Liz-Marzan, L. M.; Mulvaney, P. *Colloids Surf., A* **2002**, *202*, 119-126.

16. Osawa, M.; Ataka, K. C.; Yoshii, K.; Nishikawa, Y. *Appl. Spectrosc.* **1993**, *47*, 1497-1502.

17. McMurry, J. *Organic Chemistry*; Brooks/Cole: Pacific Grove, 1995; p 382.

18. Osawa, M.; Ikeda, M. *J. Phys. Chem.* **1991**, *95*, 99114-99119.

19. Miyake, H.; Ye, S5.; Osawa, M. *Electrochem. Commun.* **2002**, *4*, 973-977.

20. Bjerk, A.; Griffiths, R. *Anal. Chem.* **1999**, *71*, 1967-1974.

21. Gong, H.; Sun, S.G.; Li, J. T.; Chen, Y.J.; Chen, S.P. *Electrochim. Acta* **2003**, *48*, 2933-2942.

22. Doron-Mor, I.; Barkay, Z.; Filip-Granit, N.; Vashevich, A.; Rubinstein, I. *Chem. Mater.* **2004**, *16*, 3476-3483.

23. Wan, L. J.; Terashima, M.; Noda, H.; Osawa, M. *J. Phys. Chem. B* **2000**, *104*, 3563-3569.

24. Rreadeep, T.; Resmi, M. R. *J. Mol. Spectrosc.* **2000**, *202*, 303-305.

25. Zhang, Z.; Imae, T. *J. Colloid Interface Sci.* **2001**, *233*, 99-106.

26. Priebe, A.; Sinther, M.; Fahsold, G.; Pucci, A. *J. Chem. Phys.* **2003**, *119*, 4887-4890.

27. Zhang, Z.; Imae, T. *J. Colloid Interface Sci.* **2001**, *133*, 107-111.

28. Zhang, Z.; Imae, T. *Langmuir* **2001**, *17*, 4564-4568.

29. Zhang, Z.; Yoshida, N.; Imae, T.; Xue, Q.; Bai, M.; Jiang, J.; Liu, Z. *J. Colloid Interface Sci.* **2001**, *243*, 382-387.

30. Huo, S. J.; Li, Q.X.; Yan, Y. G.; Cai, W. B.; Xu, Q. J.; Osawa, M. *J. Phys. Chem. B* **2005**, *109*, 15985-15991.

31. Williams, A.; Gupta, V. K. *Thin Solid Films* **2003**, *423*, 228-234.

32. Osawa, M.; Ataka, K. I.; Yoshii, K.; Yotsuyanagi, T. *J. Electron. Spectrosc. Relat. Phenom.* **1993**, *64-65*, 371-379.

33. Krauth, O.; Fahsold, G.; Lehmann, A. *Surf. Sci.* **1999**, *433-435*, 79-82.

34. Leverette. C.; Dluhy, R. *Colloids Surf., A* **2004**, *243*, 157-167.

35. Pribe, A.; Fahsold, G.; Geyer, W.; Pucci, A. *Surf. Sci.* **2002**, *502-503*, 388-393.

36. Imae, T.; Torii, H. *J. Phys. Chem. B* **2000**, *104*, 9218-9224.

37. Miki, A.; Ye, S.; Senzaki, T.; Osawa, M. *J. Electroanal. Chem.* **2004**, *563*, 23-31.

38. Kosbar, L.; Srinivasan, C.; Afzali, A.; Graham, T.; Copel, M.; Krusin-Elbaum, L. *Langmuir* **2006**, *22*, 7631-7638.

39. Gershevitz, O; Sukenik, C. N. *J. Am. Chem. Soc.* **2004**, *126*, 482-483.

40. Duevel, R.; Corn, R. *Anal. Chem.* **1992**, *64*, 337-342.

41. Jin Lee, H.; Nedelkov, D.; Corn, R. *Anal. Chem.* **2006**, *78*, 6504-6510.

42. Nuzzo, R.; Dubois, L. W; Allara, D. *J. Am. Chem. Soc.* **1990**, *112*, 558-569.

43. Jordan, C. E.; Frey, B.L; Kornguth, S.; Corn, R. *Langmuir* **1994**, *10*, 3642-3648.

44. Nakano, K.; Yoshitake, T.; Yamashita, Y.; Bowden, E. F. *Langmuir* **2007**, *23*, 6270-6275.

45. Terrill, R.; Tanzer, T.; Bohn, P. *Langmuir* **1998**, *14*, 845-854.